Design Aspects and Characterization Tests of a Multi-Wavelength Beam HSRL for Atmospheric Monitoring in Ultra High Energy Observatories

Maragos Nikolaos*,Stavros Maltezos*, Emmanuel Fokitis*, Fetfatzis Prodromos*,Violeta Gika*,Manthos Yiannis*, Kastana Danai* and Kombitsas Michael†

*National Technical University of Athens, Greece
9, Heroon Polytechniou, ZIP 15780, Athens, Greece
†National Hellenic Research Foundation, Greece

***Abstract*. The progress in the development of a prototype High Spectral Resolution Lidar (HSRL) and the associated sub-systems for atmospheric monitoring in Ultra High Energy Cosmic Ray Observatories, will be presented in this work. In this frame, a conceptual design of a pulsed, narrow linewidth and frequency stabilized laser operating in near UV and providing multi-wavelength light beam is also described. From experimental point of view, we developed and tested the appropriate methods to characterize a commercial CW SLM Nd:YVO4 laser at 532 nm with respect of its single mode operation performance and frequency stability. Additionally, we describe the methodology and the associated results concerning the optical characterization of a candidate FabryPerot etalon being used as spectral discriminator for the molecular channel of the HSRL. For this purpose a commercial FabryPerot etalon was used as a reference to verify our results. The details of the method for accurate measurement of the effective spacing, the parallelism and the flatness of the etalons are also presented.**

***Keywords*: HSRL, LIDAR, Fabry - Perot, Laser SLM Nd:YVO4, Atmospheric monitoring**

I. Introduction

The direct detection of Ultra High Energy Cosmic Rays (UHECR) and Very-High-Energy Gamma-Rays is not efficient, mostly due to their rareness. The relevant observatories are designed to detect secondary particles produced by the interaction of the primary particle with the Earth's atmosphere. In the case of UHCRs the energy measurement is based on the calorimetric energy deposit in the atmosphere, which in turn can be measured by the emitted fluorescence light [1]. Therefore, the atmosphere can be viewed as part of the detector. Any change in atmosphere quality and its constituents can affect the signal detected. In this work we describe the design a High Spectral Resolution LIDAR (HSRL) prototype aiming to be used for the observatories mentioned above. As a source of the HSRL we consider the use of a pulsed, frequency stabilized, narrow linewidth DPSS SLM Nd:YVO_4 laser with the possibility to operate at multi-wavelength mode. For recording the backscattered signal two channels will be implemented in the receiver telescope to distinguish the aerosol signal, from the molecular one. This will be done with the use of two Fabry-Perot etalons with different mirror spacing (100 mm and 5 mm respectively). Very crucial for the performance of the HSRL are the characteristics of both the laser and the etalons. The laser it is necessary to achieve spectral stability and SLM operation while the important performance parameters of the etalons are their appropriate effective spacing, the mirror parallelism and flatness. We developed and tested appropriate methods to accomplish the above characterization. Concerning the laser, the performance tests are focused on the characterization of its frequency stability and single longitudinal mode (SLM) operation performance. The tests for the Fabry Perot etalons are focused mainly on their parallelism and flatness. An accurate and noninvasive method for determination of the effective mirror spacing of the Fabry-Perot is recently presented [2].

II. Characterization of the Nd:YVO_4 laser

A commercial CW Diode Pumped Nd:YVO_4 Single Longitudinal mode Laser at 532nm was used for the implementation of the methods, to characterize its frequency stability and mode competition. The techniques developed for this purpose are the Fringe Imaging technique (FI) and the Etalon Scanning technique (ES).

The FI technique is based on the analysis of the geometrical characteristics of recorded interference fringe images. In detail in the FI technique, the light after passing throe a Fabry-Perot etalon is focused in a screen (CCD) producing a series of interference fringes at angles θ_m from the normal to the etalons plates [3]. Were

$$cos(\theta_m) = \frac{m\lambda}{2d} \quad (1)$$

(d) is the distance between the etalons mirrors, (λ) the wavelength of the analyzed light and (m) is an integer witch defines the order of interference and has a maximum value $m_0 = int(\frac{2d}{\lambda})$. By determining the

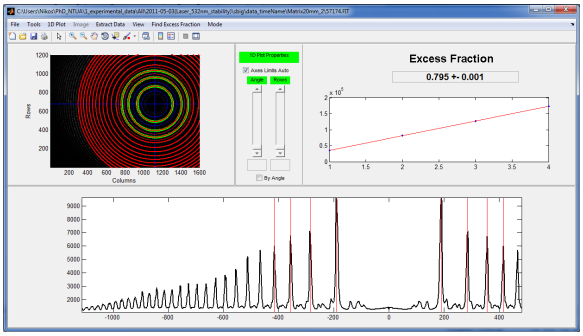

Fig. 1: MATLAB Program for the analysis of interference fringe images.

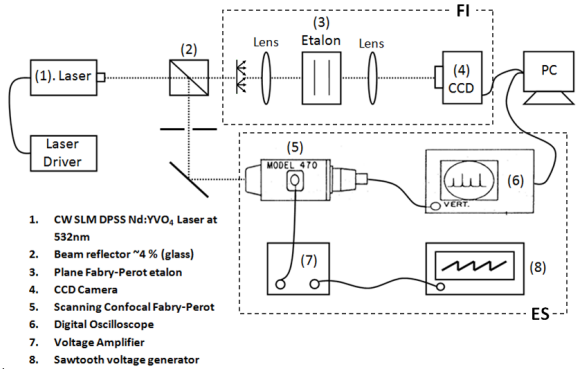

Fig. 2: The experimental setup for the characrerisation of the Nd:YVO_4 Laser.

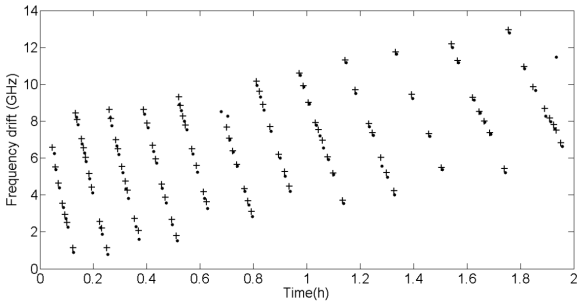

Fig. 3: Plot of the rate of the frequency drift vs the elapsed time from the moment the laser started to operate.

radius of at least two fringes of the fringe pattern, we can determine the related Excess Fraction (ϵ) witch is the fractional part of $\frac{2d}{\lambda}$. Variations of the Excess Fraction can be translated in frequency variation within the Free Spectral Range (FSR) of the etalon.

$$\Delta f = \frac{c}{2d}\Delta\epsilon \tag{2}$$

For the analysis of the digital CCD fringe images we developed an appropriate Matlab program. This program extracts the related fringe radii and correlates them with the corresponding Excess Fractions (Fig. 1), which in turn are related to the frequency variation of the laser.

The ES technique is based on recording interference variations by a scanning Fabry-Perot interferometer. In detail a Fabry-Perot interferometer is used with one of its mirrors attached to a piezoelectric material. By applying a sawtooth voltage ($V(t)$) to the material we can periodically and in a linear matter change the distance between the mirrors within a certain range $[d_{min} - d_{max}]$. Using a photodiode we can monitor the intensity of the light at angle $\theta = 0$ after the interference of the multi-reflected beam. This signal can be seen with the help of an oscilloscope triggered with respect to the sawtooth voltage. As a result we can see a series of intensity peaks whose positions in the oscilloscope time axis (x) reflect the mirrors spacings at witch constructive interference occurs. Frequency variations, thus variations of the Excess Fraction are analogous to variations in peaks positions:

$$\Delta\epsilon = \frac{\Delta x}{\Delta x_{FSR}} \tag{3}$$

, were Δx_{FSR} is the distance between two intensity peaks produced by successive orders of interference.

III. Experimental setup and Data

The related experimental setup is illustrated in Figure (2). The laser beam is splitted in two by a glass reflector. The resulting beams are analyzed by either the FI or the ES technic. For the FI technic we used a commercial 5 mm plane etalon with near 20 GHz FSR. For the ES technic a commercial confocal scanning Fabry-Perot of 2 GHz FSR (model 470 of Spectra Physics [4]) was used in combination with a digital oscilloscope. A first series of data have been taken with the laser cooled by a solid metal with small air-exposed surface. Both techniques were used simultaneously and cross-checked for any systematic errors. Subsequent CCD images and oscilloscope snapshots were taken for a near two hour time period and analyzed to extract the Frequency drift of the laser due to its temperature rising. The resulting data are shown in fig. 3. We can see that both methods agree showing that mode hopping occurs every about 8GHz of frequency drift.

A second series of data have been taken with the laser cooled by an aluminium heat sink. Only the FI method is used this time, with an 20 mm etalon for higher spectral resolution. The frequency drift versus time is presented in figure 4. Mode hopping occurs only ones after about 1.5 hour of operation and after tree hours the laser reaches near an equilibrium, were the frequency is starting to oscillate around a central value.

Conclusions about the evolution of the mode structure can be made from the one-dimensional intensity plots of the fringe patterns at several times within the monitoring period, illustrated in figure 5. It can be seen that for the first 1.5 hours many modes oscillate in the laser cavity. Only after 1.5 hours the laser becomes SLM.

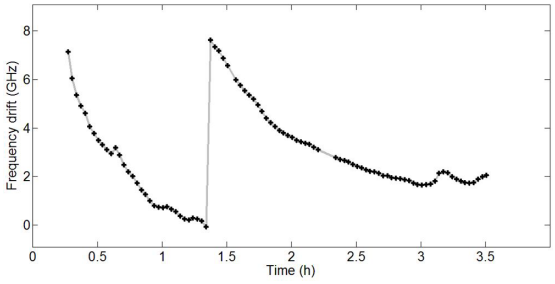

Fig. 4: Plot of the relative Frequency of the most intensive laser mode vs. the elapsed time from the moment the laser started to operate.

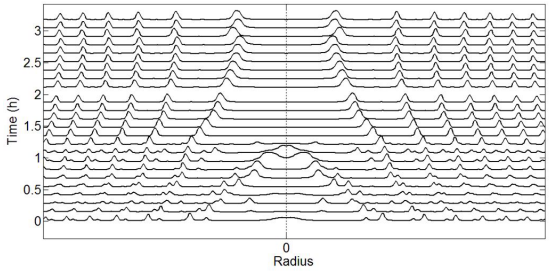

Fig. 5: One dimentional intensity plots of the fringe paterns shifted at an amound equal to the time they were taken.

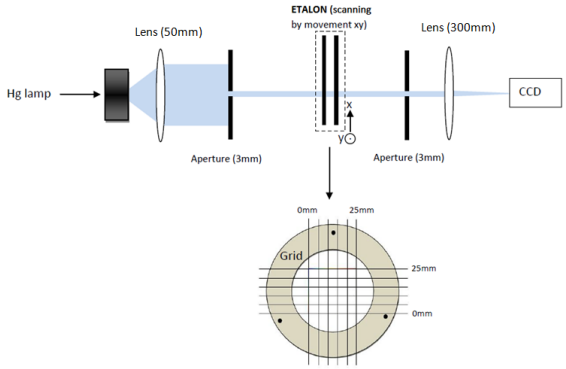

Fig. 6: Experimental setup for the characterization of the Fabry-Perot etalon with respect to its Flatness.

IV. Etalon Flatness Determination

The parallelism and the overall flatness (or Peak-to-Valley) of the etalon plates is crucial for its performance. We have applied a simple but effective method to characterize a prototype Fabry-Perot etalon along with a commercial one with respect to these features. This method is based in restricting the operational surface of the etalon plates to a small spot with radius of a few millimeters. This lets us measure the etalon characteristics in different parts of its surface, mapping the hole surface. The experimental setup we used is illustrated in figure 6. As a light source we used the 435nm spectral line of a Hg lamp. The restriction of the etalons operational surface is achieved with two 3mm apertures at both sides of the etalon. The etalon is placed on a mechanical

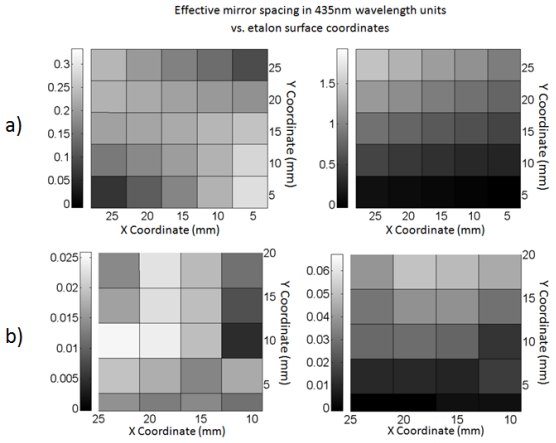

Fig. 7: Right: Map of the effective etalon spacing in units of 435 nm wavelength (gray scale) . Left: Map of the effective etalon spacing with deviation from parallelism removed to reveal the etalons flatness. a) Prototype 13 mm etalon b) Commercial 5 mm etalon.

support to control its movement in the xy plane, bringing the spot to the desired coordinates of the grid, shown in figure 6. For every grid poind a interference fringe image is taken with the CCD camera. The images are analyzed to extract the related excess fractions at every grid poind. The variations of the excess fractions ($\Delta\epsilon$) from point to point are translated in variation in the effective distance between the etalon plates.

$$m + \epsilon = \frac{2d}{\lambda} \Rightarrow \Delta d = \frac{\lambda}{2}\Delta\epsilon \qquad (4)$$

At Fig. 7 we illustrate the experimental data for both etalons. For the prototype etalon (upper graphs) we can see that the overall flatness (Peak to Valley) for a 25 x 25 mm surface is of the order of $\lambda/4$ (left graph). Reducing the surface of operation we can achieve better flatness. The angle between the etalons plates can be derived from the right graph. We can see that the etalon spacing in the upper left corner of its plate differs from that of lower right corner more than 1.5λ. This means that the spacers need adjustments to achieve better parallelism. The overall flatness of the commercial etalon (lower graphs) is of the order of $\lambda/40$

References

[1] F. Arqueros, F. Blanco, A. Castellanos, M. Ortiz and J. Rosado, *The yield of air fluorescence induced by electrons*, http://arxiv.org/PS_cache/astro-ph/pdf/0604/0604498v2.pdf (2006).

[2] S. Maltezos, N. Maragos, E. Fokitis, V. Gika, A. Georgakopoulou, E. Koubli and G. Koutsourakis, *High-Accuracy Determination of Fabry-Perot Effective Mirror Spacing used for the Receivers of Atmospheric Monitoring in VHE Gamma Ray Astronomy*, 12th ICATPP Como, Italy (2010).

[3] J. M. Vaughan, Adam Hilger, *The Fabry-Perot Inteferometer*, Series on Optics and Optoelectronics.

[4] J. Kauppinen, *A Simple Method for Single-Frequency Operation and Stabilization of a He-Ne Laser*, Appl. Phys. B 26, 193-195 (1981).